Collision Time Measurements in a Sonoluminescing Microplasma with a Large Plasma Parameter

A. Bataller,* B. Kappus, C. Camara, and S. Putterman
[1]Department of Physics and Astronomy, University of California, Los Angeles, Los Angeles, California 90095, USA
(Received 29 March 2014; published 7 July 2014)

The plasma which forms inside of a micron-sized sonoluminescing bubble in water for under a nanosecond has been probed with 3 ns long laser pulses. A comparison of the response to 532 and 1064 nm light indicates that the plasma number density is about 2×10^{21} cm^{-3} and that transport properties are dominated by strong screening and correlation effects. The spherical shape, well-defined atomic density, and blackbody temperature make the sonoluminescing plasma a test bed for theories of strongly coupled plasmas. The plasma in this experiment distinguishes between competing theories of strong, intermediate, and weak effective screening.

DOI: 10.1103/PhysRevLett.113.024301 PACS numbers: 43.35.Hl, 52.27.Gr, 52.38.−r, 78.60.Mq

The passage of a planar sound wave through a fluid leads to pulsations of a trapped bubble that are so large that the energy density of sound is concentrated by 12 orders of magnitude to generate flashes of ultraviolet light that can be as short as 35 ps [1–3]. The mechanism of energy concentration and the state of the bubble contents at the moment of light emission constitute the study of sonoluminescence (SL). During the rarefaction part of the sound field, the radius R of the bubble expands to a maximum value, where the internal pressure of the gas it contains is low compared to the ambient value of 1 atm. In a 30 kHz sound field, the subsequent implosion is supersonic as it passes through the ambient radius R_0 on the way to a collapse radius R_c [4]. The ideal gas law gives an ambient density of $n_0 = 2.4 \times 10^{19}$ cm^{-3} and for xenon gas $R_0/a \sim 7.6$, where a is the radius of the bubble when the gas is compressed all the way to its van der Waals hard core. Light scattering measurements indicate that for a trapped single bubble in a 30 kHz sound field, $R_c \sim a$, so that the atomic density in the collapsed xenon bubble is $n_c \sim 10^{22}$ cm^{-3} [5].

At the moment of maximum compression, $R \sim R_c \sim 1/2$ μm, a flash of light is emitted. Its spectral density closely matches an ideal Planck blackbody [6–9]. As a blackbody is opaque, the free charge density must be very high. According to the simplest formulas for opacity, where it is due to scattering of light by free charges [10], a photon mean free path of $1/2$ μm at 532 nm and the measured temperature of 9250 K requires a charge density $n_e > 10^{21}$ cm^{-3}. Analysis of line spectra in other sonoluminescing systems has been interpreted in terms of similar charge densities and temperatures [11–13].

The repetitive attainment of such dense plasmas in spherical geometries with a controlled atomic density at temperatures $T \sim 1$ eV enables the use of SL for studying transport properties of dense plasmas. For this case, the plasma coupling parameter is $2.9 < \Gamma < 6.3$, where

$$\Gamma = \frac{e^2}{kT}\left(\frac{4\pi n_e}{3}\right)^{1/3}. \quad (1)$$

In this Letter we explore this new direction in SL research by comparing the response of the SL plasma to input laser light at two different wavelengths, 1064 and 532 nm. This test is motivated by the fact that the free charge densities are so high that the corresponding plasma frequency $\omega_p = \sqrt{4\pi n_e e^2/m}$ (where m is the electron mass) is comparable to the angular frequency ω of the light in the laser pulses, which can be used to probe the SL microplasma. According to whether $\omega > \omega_p$ or $\omega < \omega_p$ the incident light is transmitted or reflected by an ideal plasma. We note that $n_e \sim 10^{21}$ cm^{-3} corresponds to a plasma wavelength $\lambda_p \sim 1000$ nm, which lies between the 1064 and 532 nm probe pulses. The goal of studying the interaction of a laser with SL was first introduced by Diebold [14] with the purpose of generating high plasma temperatures. A recent experiment by Khalid *et al.* [15] demonstrated successful SL-laser coupling and provided further evidence that SL arises from a highly ionized plasma [13,16]. Our experiment entails both spatial and temporal challenges. The laser must hit the bubble at a properly synchronized moment during the acoustic cycle.

Figure 1 shows the main experimental observation that (a) a weak pulse of 532 nm light can interact with the SL plasma and lead to an increase in light emission, whereas (b) the 1064 nm light interacts with the SL plasma only above an intensity threshold. The upper data set on each panel shows the Mie scattering signal from the bubble, which is a measure of its radius. The lower curve shows the intensity of SL during that same acoustic cycle as recorded by a photomultiplier tube (PMT). The diagonal data set in the middle shows the increase in light output of the bubble when the laser hits the bubble during the lifetime of the SL microplasma. Theoretical analysis of this data permits one

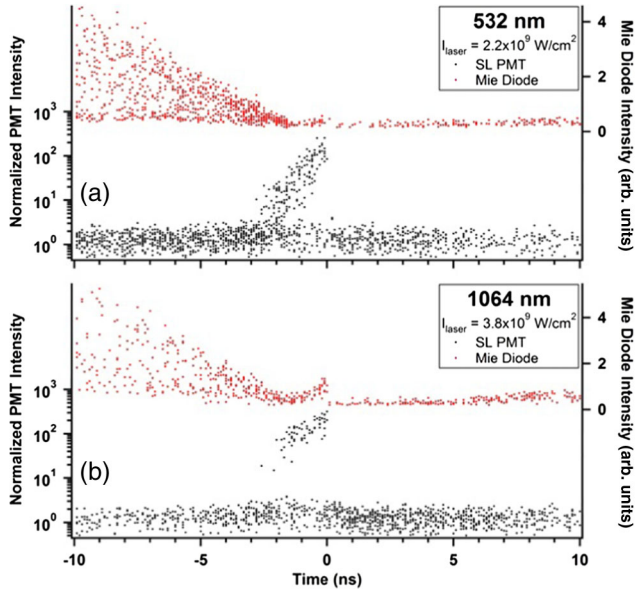

FIG. 1 (color online). Scatter plots showing the Mie scatter intensity (red dots) and the SL intensity (black dots) for (a) 532 and (b) 1064 nm. The SL intensity is normalized by the intensity distribution of SL flashes without an incident laser pulse and can be seen as a band of points centered on unity. For each SL intensity point, there is a corresponding Mie scatter point which is a measure of the bubbles' radius and confirms successful spatial synchronization. SL-laser interactions only occur when the laser and SL flash overlap in time. The spread in Mie scatter points is due to the drift in bubble location relative to the laser focus during the laser's repetition rate (10 Hz). As SL-laser interactions grow stronger, the accompanying Mie scatter signal increases due to an enlarged plasma radius.

to select between the transport theory of dilute plasmas and various density modifications put forward by different authors [17–19].

Into degassed water we dissolve 150 torr of a gas mixture that is 99% nitrogen and 1% xenon. The water is in a 30 kHz quartz resonator driven by piezoelectric transducers. A bubble is seeded into the resonator near the velocity node of the standing wave resonance and is driven to large pulsations and sonoluminescence. A seeded YAG (TEM00) laser is synchronized with the bubble by timing from the previous SL emissions, as the flashes have a subnanosecond clocklike repetition [20]. Three light detectors are used: a photodiode which records the scattered laser light, a photodiode that measures the intensity and timing of the laser pulse, and a PMT with a laser-blocking filter (Notch) that records the broadband SL as well as the additional broadband emission which results from a laser pulse that is successfully synchronized with a SL flash. The acquisition of many scattering events and many flashes of SL is displayed in Fig. 1. The intensities of each event are plotted as a function of the time elapsed between the leading edge (10% peak intensity) of the laser pulse and the SL flash (which occurs at $t = 0$). For instance, the SL events plotted at -4 ns (on the lowest trace) correspond to acoustic cycles where the leading edge of the laser hit the bubble 4 ns before the SL flash. Such an early hit corresponds to a bubble with a radius larger than R_c, and so the laser light scattered from the bubble as shown on the upper trace is much larger than occurs at the minimum radius, which happens at $t = 0$. If the bubble is not at its minimum radius, i.e., if it is not in the process of emitting SL, then the PMT records the intensity of the SL flash for that cycle and it is plotted below the time of the laser hit. This is shown by the PMT events close to the abscissa. As the laser pulse is $\sim$3 ns in duration, a laser-plasma interaction can occur even when the leading edge of the laser reaches a bubble 3 ns before SL. These laser on plasma events can be weak (532 nm) or zero (1064 nm) because the laser is turning off as the SL is turning on. A laser hit can also result in a weak interaction if the bubble is not centered on the laser's focus, which results in a spread in Mie intensities for a given time. Because of the maximum available pulse energy, the largest events are seen when the laser arrives at the bubble as SL is turning on. In this case, we find broadband emission with an energy that can be much higher than a typical flash of SL.

The SL-laser interaction gap (see Fig. 1) for 532 vs 1064 nm is apparent in the histogram of events shown in Fig. 2. Figure 2 displays the frequency of events during the SL-laser temporal overlap as a function of the intensity of total light emission from the bubble. This includes the usual SL plus the energy grabbed from the laser by the SL plasma. The peak at unity is the strength of a typical free running flash of SL and the gap from 4–20 reflects the difference in interaction of the 532 vs 1064 nm laser wavelengths with the SL plasma. What we measure is clearly below the breakdown threshold which occurs at an intensity 50 000 times that of SL and 200 times larger than the minimum observable laser bubble interaction. This

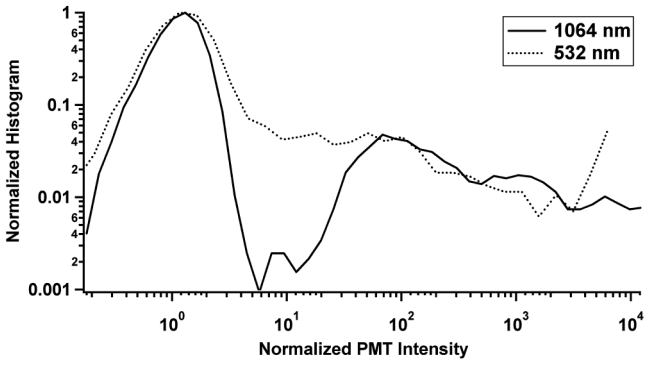

FIG. 2. Normalized histogram of the SL intensity for a range of laser intensities (0.5–25 $\times$ 10^9 W/cm^2) at 1064 (solid curve) and 532 nm (dotted curve). Only points within the interaction region of -4 to $+1$ ns (532 nm) and -8 to $+1$ ns (1064 nm) were used for the histogram. Although concurrent to the SL, a large number of laser shots did not result in an interaction due to the lack of spatial overlap caused by the bubbles' drift in location.

confirms that we are seeing an interaction between the laser and the SL plasma.

The interaction of a laser pulse with a plasma is affected by the plasma frequency and the collisionality (or absorptivity) of the plasma. The reflection of light by a sufficiently dense plasma when $\omega < \omega_p$, assumes an ideal plasma with $\omega\tau \gg 1$, where τ is the collision time. In this limit the motion is reversible and no energy is absorbed by the plasma. A theory which explains the conversion of incoming light into plasma energy must include a finite τ.

Reflectivity in the limit $\tau \to \infty$ is graphed in Fig. 3. The solid curves give the plasma reflectance as a function of the free charge density for 532 and 1064 nm. On Fig. 3 this is labeled as the Debye theory of transport. The transition to complete reflectance at high charge density is the well-known plasma frequency effect which motivated this experiment. When interactions are included according to the transport theory of a dilute plasma (see below), one obtains the dotted line in Fig. 3. Application of the theory of dilute plasmas to high charge densities leads to short collision time, $\omega\tau < 1$. In this limit absorption shorts out plasma reflection. An explanation of the SL-laser interaction requires a theory of the collision time for dense plasmas which follows.

Electrons of mass m and velocity $\vec{v}$ are accelerated by an electric field $\vec{E}$ according to the Drude model,

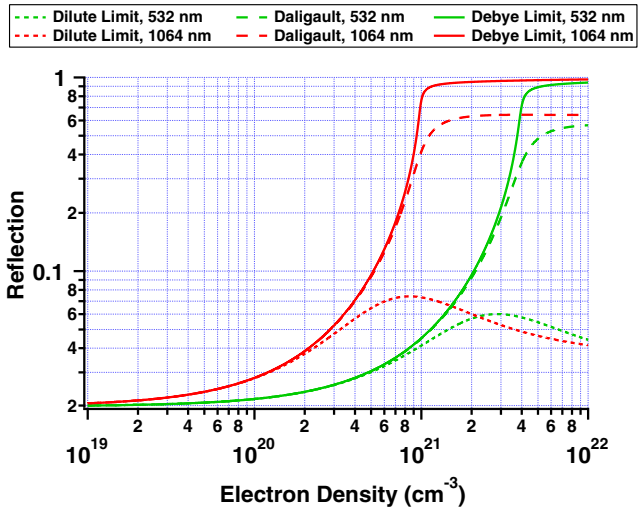

FIG. 3 (color online). Plasma reflection of 532 and 1064 nm light as a function of electron density for various collision theories. The Debye theory (solid curves) represents a highly screened plasma, where $\omega\tau \gg 1$ and high levels of reflection are observed for $\omega < \omega_p$. The dilute theory (dotted curves) diverges from the high reflectivity behavior due to strong damping ($\omega\tau \lesssim 1$) in the high density regime. The Daligault theory (dashed curves) experiences an intermediate level of reflection in the dense regime and is capable of describing both reflection at 1064 nm and spectral opacity at 532 nm.

$$m\frac{d\vec{v}}{dt} + \frac{m}{\tau}\vec{v} = -e\vec{E}. \tag{2}$$

When coupled to Maxwell's equations in the presence of a disturbance driven at frequency ω, one obtains the dispersion law for the plasma wave number k_p given by [21]

$$k_p^2 = \frac{\omega_p^2}{c^2}\frac{i\omega\tau}{1 - i\omega\tau} + \frac{\omega^2}{c^2}. \tag{3}$$

For the frequency dependent collision time in the gaseous plasma, we take

$$\tau = \frac{3\hbar\omega}{4\pi n_e e^4[1 - e^{-\beta\hbar\omega}]}\sqrt{\frac{3mkT}{2\pi}}\frac{1}{\ln\Lambda}. \tag{4}$$

This term includes the limit of $\hbar\omega \to 0$, where τ is determined by small energy collisions in a Coulomb plasma, as well as free-free scattering in which an electron absorbs a photon of frequency ω. In the limit where $\omega > \omega_p$, $\omega\tau \gg 1$, and $\ln\Lambda = 1$, Eqs. (3) and (4) yield a $2\mathrm{Im}(k_p)$ consistent with inverse bremsstrahlung attenuation of light (Eq. 5.21 of [10] corrected for induced emission).

For a strongly coupled plasma (SCP) where $\Gamma > 1$, screening and correlations must be included to determine the effective collision frequency. Particle interactions are well described in the framework of binary collisions, even in the dense plasma limit [22]. In this spirit, we present a simplified theory where the effects of SCPs are included in our choice of the collision time. For this analysis, we consider three models that assign a formulation for the Coulomb logarithm in Eq. (4). The first is an extreme screening model that utilizes the logarithmic formulation presented by Valuev [17] and sets the Debye length as the maximum impact parameter [Eq. 5(a)]. The second model proposed by Daligault [18] represents an intermediate scaling of the impact parameter [Eq. 5(b)] and includes correlation effects. The dilute theory is also considered for comparison [Eq. 5(c)], where screening is weak and held constant. These models are given by

$$\text{Debye:}\quad \ln\Lambda = \frac{\sqrt{3}}{\pi}\ln\sqrt{\frac{1}{6}\Gamma_\omega^{-3} + 1}, \tag{5a}$$

$$\text{Daligault:}\quad \ln\Lambda = \frac{\sqrt{3}}{\pi}\ln\left(\frac{0.7}{\sqrt{6}}\Gamma_\omega^{-3/2} + 1\right), \tag{5b}$$

$$\text{Dilute:}\quad \ln\Lambda = \frac{\sqrt{3}}{\pi}, \tag{5c}$$

where

$$\Gamma_\omega = \Gamma\left(\frac{kT}{\hbar\omega}(1 - e^{-\beta\hbar\omega})\right). \tag{6}$$

As we apply transport theory over a range of frequencies we include the possibility of the plasma coupling parameter becoming a function of frequency [Eq. (6)] as has been included by Dawson [23]. Furthermore, we have also included an overall factor of ~2 in Eq. (4) that distinguishes Dawson and Daligault from Zel'dovich.

Strong effective screening [Eqs. 5(a) and 5(b)] lengthens the collision time for $\Gamma > 1$, and, according to Eq. (6), this effect varies with wavelength. Figure 4 shows the distance light travels before decaying to $1/e$ as a function of electron density for the Daligault theory [Eq. 5(b)]. The region labeled τ dominated occurs when the laser frequency is greater than the plasma frequency. For the Daligault theory at a charge density of $\sim 2 \times 10^{21}$ cm^{-3}, the 532 nm light is τ dominated while the 1064 nm light is ω_p dominated and is strongly reflected. In this range of charge density, the 532 nm penetrates most of the bubble while the 1064 nm penetrates just a fraction of the bubble radius.

We appeal to the Daligault theory and the region of parameter space with a charge density of $\sim 2 \times 10^{21}$ cm^{-3} to explain the interaction of a laser with the microplasma in a sonoluminescing bubble. First, at this density the decay length of 532 nm light is approximately equal to the bubble radius which is consistent with the observed Planckian spectrum. Next, the 532 nm light penetrates the bubble whereas the 1064 nm light is restricted to a depth less than 20% of the bubble radius. Furthermore, the intensity of light at 1064 nm to penetrate into the surface region is down by a factor of 2.5 from the 532 nm light. It is important to note that for all of the theories discussed, densities lower than 10^{21} cm^{-3} would result in weak laser-plasma coupling due to the long decay length (Fig. 4).

A full explanation of the absorption gap shown in Figs. 1 and 2 still requires some nonlinear threshold phenomenon that allows for weak interactions at 532 nm but precludes the absorption of weak laser light at 1064 nm. This phenomenon goes beyond processes that we have included in the theory of τ (Fig. 5). To this end we note that the average laser intensity at 1064 nm is 3.8×10^9 W/cm^2, which corresponds to an electric field $E \sim 10^6$ V/cm. From Fig. 5 the collision time is about 5 fs so that between collisions, an electron with thermal velocity $\sim 7 \times 10^7$ cm/s moves about 3.5 nm. The change in electron velocity during a period of light is about 10^6 cm/s. The number of velocity increments of this size required to double the energy is 50, if the collisions were all additive. Because of the randomness of collisions and due to $\omega\tau \sim 4$, the total number of collisions required to double the energy is $50 \times 50 \times 4 \times 4 = 40\,000$. During this time the electron walks a distance ~1 μm. This distance is much greater than the electric fields' penetration depth, which we interpret as implying that at 1064 nm, externally driven diffusion precludes finite energy transfer. At 532 nm the response is τ dominated and the field penetrates most of the bubble and finite transfer is possible. The time required for the energy of an electron to double in the externally applied field is about 0.5 ns. Possible threshold phenomena include breakdown at the water interface and higher levels of ionization.

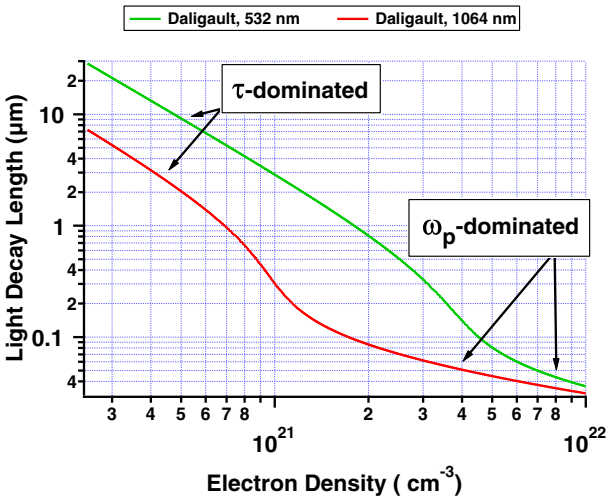

FIG. 4 (color online). Decay length of light in a dense plasma for 532 and 1064 nm using the collision theory of Daligault. Two absorption regimes are present for the electron density under consideration and are separated at the critical density ($\omega_p = \omega$). Based on the suggested electron density of $\sim 2 \times 10^{21}$ cm^{-3} for the SL measured in this experiment, the absorption is τ dominated for 532 nm and ω_p dominated for 1064 nm.

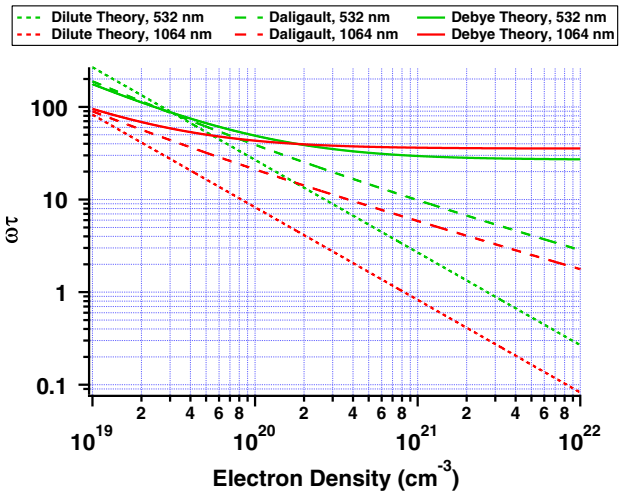

FIG. 5 (color online). Collision time of 532 and 1064 nm light as a function of electron density for various collision theories. The collision time for the Debye theory (solid curves) is large for all electron densities and becomes density-independent for large plasma parameters. The dilute theory (dotted curves) represents the shortest collision time. The intermediate theory of Daligault (dashed curves) lies between these limiting theories and scales with ω_p for large densities.

The plasma which forms in a collapsing noble gas bubble reaches a density with a plasma coupling parameter in excess of unity. The bubble has a well-defined number of atoms, a blackbody temperature, and is spherical in shape. It therefore becomes a test bed for the study of transport phenomena in dense plasmas. We have probed the sonoluminescing micro-plasma by targeting it with synchronized laser pulses at 532 and 1064 nm. Light emissions from the resulting interactions enable one to decide between various transport theories of dense plasmas and to determine that the plasma density is about $2–3 \times 10^{21}$ cm^{-3}. This technique has provided an electron density measurement for single-bubble SL in water, which has remained elusive for almost 25 years after its discovery. The measured plasma density of $\sim 3 \times 10^{21}$ cm^{-3} corresponds to a Fermi temperature of 8700 K, which is slightly less than the spectral temperature. The possibility remains that some regions of the SL parameter space can exhibit Fermi degeneracy as well as dense plasma kinetics [24,25].

We gratefully acknowledge support from DARPA MTO for research on microplasmas and AFOSR for research on transport in dense plasmas. We thank Guillaume Plateau and Keith Weninger for valuable discussions.

*bataller@physics.ucla.edu

[1] R. Hiller, S. J. Putterman, and B. P. Barber, Phys. Rev. Lett. **69**, 1182 (1992).
[2] B. Gompf, R. Günther, G. Nick, R. Pecha, and W. Eisenmenger, Phys. Rev. Lett. **79**, 1405 (1997).
[3] R. Hiller, S. J. Putterman, and K. R. Weninger, Phys. Rev. Lett. **80**, 1090 (1998).
[4] K. R. Weninger, B. P. Barber, and S. J. Putterman, Phys. Rev. Lett. **78**, 1799 (1997).
[5] B. P. Barber, R. A. Hiller, R. Löfstedt, S. J. Putterman, and K. R. Weninger, Phys. Rep. **281**, 65 (1997).
[6] G. Vazquez, C. Camara, S. Putterman, and K. Weninger, Opt. Lett. **26**, 575 (2001).
[7] C. Camara, S. Putterman, and E. Kirilov, Phys. Rev. Lett. **92**, 124301 (2004).
[8] D. J. Flannigan and K. S. Suslick, Nature (London) **434**, 52 (2005).
[9] S. Hopkins, S. Putterman, B. Kappus, K. Suslick, and C. Camara, Phys. Rev. Lett. **95**, 254301 (2005).
[10] Ya. B. Zel'dovich and Yu. P. Raizer, *Physics of Shock Waves and High-Temperature Hydrodynamic Phenomena* (Dover, New York, 1966).
[11] K. S. Suslick and D. J. Flannigan, Annu. Rev. Phys. Chem. **59**, 659 (2008).
[12] D. J. Flannigan and K. S. Suslick, Nat. Phys. **6**, 598 (2010).
[13] B. Kappus, S. Khalid, A. Chakravarty, and S. Putterman, Phys. Rev. Lett. **106**, 234302 (2011).
[14] G. Cao, S. Danworaphong, and G. J. Diebold, Eur. Phys. J. Spec. Top. **153**, 215 (2008).
[15] S. Khalid, B. Kappus, K. Weninger, and S. Putterman, Phys. Rev. Lett. **108**, 104302 (2012).
[16] B. Kappus, A. Bataller, and S. Putterman, Phys. Rev. Lett. **111**, 234301 (2013).
[17] Y. K. Kurilenkov and A. A. Valuev, Contrib. Plasma Phys. **24**, 161 (1984).
[18] G. Dimonte and J. Daligault, Phys. Rev. Lett. **101**, 135001 (2008).
[19] S. A. Khrapak, Phys. Plasmas **20**, 054501 (2013).
[20] B. P. Barber and S. J. Putterman, Nature (London) **352**, 318 (1991).
[21] S. Eliezer, Plasma Phys. Controlled Fusion **45**, 181 (2003).
[22] S. D. Baalrud and J. Daligault, Phys. Rev. Lett. **110**, 235001 (2013).
[23] T. W. Johnston and J. M. Dawson, Phys. Fluids **16**, 722 (1973).
[24] S. Ichimaru, Rev. Mod. Phys. **54**, 1017 (1982).
[25] S. Ichimaru, *Statistical Plasma Physics, Volume I: Basic Principles*, Frontiers in Physics Series (Westview, New York, 2008).